ACS APPLIED MATERIALS & INTERFACES

LETTER

www.acsami.org

Flexible and Semitransparent Strain Sensors Based on Micromolded Pd Nanoparticle−Carbon μ-Stripes

B. Radha, Abhay A. Sagade, and G. U. Kulkarni*

Chemistry and Physics of Materials Unit and DST Unit on Nanoscience, Jawaharlal Nehru Centre for Advanced Scientific Research, Jakkur P.O., Bangalore 560064, India.

Supporting Information

ABSTRACT: Flexible resistive strain sensors have been fabricated by micromolding Pd alkanethiolate on polyimide substrates and subjecting to thermolysis in air. Thus produced stripes were ∼1 μm wide with spacing of ∼0.5 μm and contained Pd nanoparticles in carbon matrix. The nanoparticle size and the nature of carbon are much dependent on the thermolysis temperature as is also the resistance of the microstripes. Generally, lower thermolysis temperatures (<230 °C) produced stripes containing small Pd nanoparticles with significant fraction of carbon from the precursor decomposition. The stripes were poorly conducting yet interestingly, exhibited change of resistance under tensile and compressive strain. Particularly noteworthy are the stripes produced from 195 °C thermolysis, which showed a high gauge factor of ∼390 with strain sensitivity, 0.09%. With molding at 230 °C, the stripes obtained were highly conducting, and amazingly did not change the resistance with strain even after several bending cycles. The latter are ideal as flexible conduits and interconnects. Thus, the article reports a method of producing flexible sensitive strain sensors on one hand and on the other, flexible conduits with unchanging resistance, merely by fine-tuning the precursor decomposition under the molding conditions.

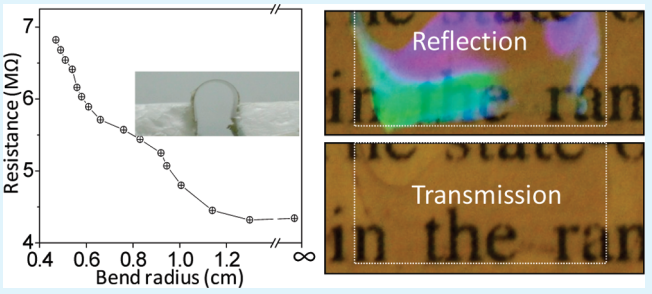

KEYWORDS: strain sensor, micromolding, palladium, interconnect, bending, carbonaceous matrix

INTRODUCTION

Flexible electronics, in contrast to conventional electronics, make use of material components with a wide range of response to bending, stretching, or twisting; they either respond sensitively or strive to remain constant.[1] Although those responding are to be found in device parts such as touch screen, the latter are important in conduits and interconnects. In a laboratory setting, the strain gauge factor distinguishes the two performances. The gauge factor for a resistive sensor is the relative change in its resistance divided by the strain applied.[2] Obviously in a flexible circuit, the conduits and interconnects are expected to exhibit near zero gauge factor over repeated bending, unlike user interface components for which high gauge factors are desirable.[3,4] The literature is abundant with examples of both classes of materials. Based on constant resistance interconnects, Rogers and co-workers fabricated foldable inorganic light emitting diodes on a PET substrate capable of functioning at bent radii down to 0.7 mm with no change in performance.[5] Likewise, GaN high electron mobility transistors,[6] graphene FETs,[7] GaAs MESFETs,[8] solar cells,[9,10] photodetectors,[11] resistance switching memory devices,[12] nanogenerators,[13,14] ultrahigh frequency electronics,[15] etc., have been fabricated on flexible substrates. Stretchable and transparent carbon nanotube thin films have been fabricated that sustain extremely large strains.[16] Transparent conducting electrodes for organic solar photovoltaics have been made using graphene on a PET substrate where, the conductance of the electrodes decreased by only 7.9% after 100 bending cycles.[17] Various semiconductor nanostructures have also been explored for the purpose of high performance flexible electronics.[18] Controlling the buckling of Si nanowires, stretchable conduits were realized.[19]

The sensors with high strain gauge factors are important in flexible electronics as well as in stand-alone devices. The latter have been in use for structural health monitoring[20] of critical infrastructures−highways, buildings, bridges, aircraft, ships, and pipelines, particularly during earthquakes, hurricanes, and other natural disasters. As regards resistive sensors (capacitive sensors and optical sensors being examples of other types of strain sensors), thin metal films have served as strain gauges for decades,[21] and recently bimetal alloys (e.g., Ni−Ag,[22] Ni−Cr[23]) have replaced them for want of better adherence and corrosion resistance. Fiber-concrete composites[24] are yet another class of strain sensors. Microcrystalline and amorphous Si strain sensors are also well-known.[25] Conducting polymer based sensors have been developed[26] and in another example, conductive-polymer strain sensors for touch input sheets have been fabricated which are sensitive to bending radius of 20 mm.[27] In this context, several

Received: March 7, 2011
Accepted: May 6, 2011
Published: June 17, 2011

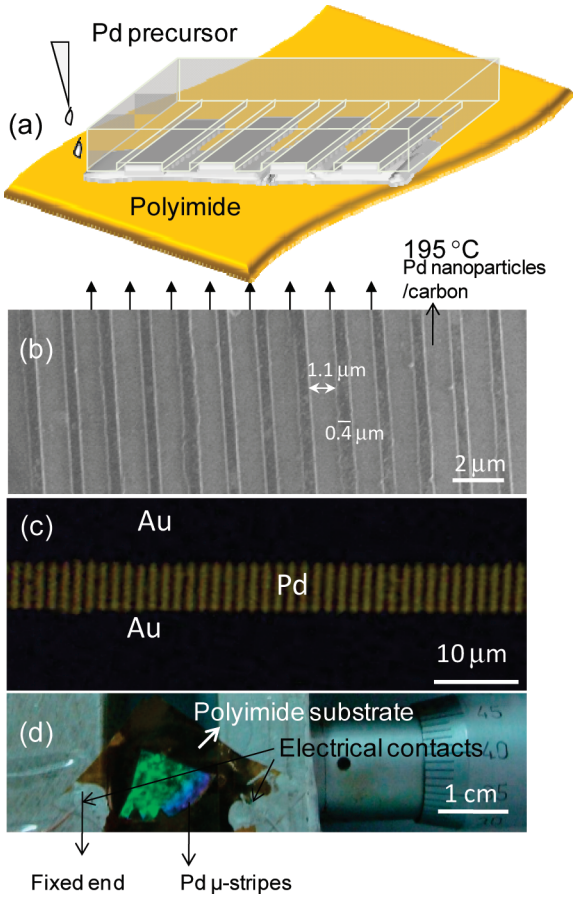

Figure 1. (a) Schematic showing direct micromolding of Pd hexadecylthiolate onto a polyimide substrate. (b) SEM image of the formed stripes on polyimide substrate. (c) Optical image of the Pd μ-stripes across the Au electrodes. (d) Photograph of the device used for bending experiments. The color from diffraction of ambient light by the μ-stripes may be seen.

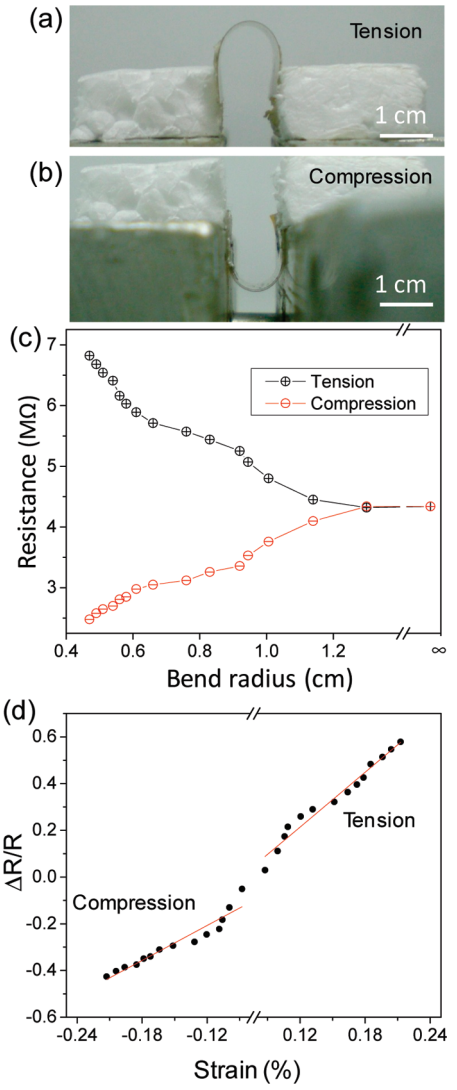

Figure 2. Digital photographs of the device with Pd μ-stripes (thermolysis temperature, 195 °C) under (a) tension and (b) compression. One end of the device was moved with the aid of a screw gauge (see Figure 1d), whereas the other end was held fixed. (c) Variation in resistance with bend radius during tension and compression. (d) Normalized change in resistance as a function of strain. The % strain (ε) was calculated as $\varepsilon = d/2r$,[25] d being the substrate thickness and r the radius of curvature.

nanomaterials are being projected for highly sensitive sensors. Single ZnO nanowire,[3] single-walled carbon nanotubes,[28] networked Au nanoparticle coatings,[27] self-assembled monolayers of nanoparticles,[30,31] have served as sensor elements. Bridging ZnO nanorods into circuits, strain driven transistors have been fabricated with high on−off ratios particularly at strains >1.4%.[32] ZnO embedded paper composite is shown to work as strain sensor with a gauge factor of ~21.[33] Here, we report the fabrication and performance of Pd nanoparticle based micro-(μ)-stripes patterned directly on a flexible substrate, which based on the heat treatment employed during patterning, serve as highly sensitive strain sensor or as reliable conduits. Previously, we have reported a method of molding metallic Pd μ-stripes and nanowires onto flat rigid substrates such as Si, by direct micromolding in capillaries.[34] In the present work, we have molded the Pd nanoparticle stripes on a flexible polyimide substrate under varying thermolysis conditions, in order to realize the strain sensing action. Thus produced sensor device is highly sensitive and reasonably transparent.

RESULTS AND DISCUSSION

Pd μ-stripes were patterned onto a flexible polyimide substrate by direct micromolding. Pd hexadecylthiolate in toluene (10 mM) served as a precursor for molding using a polydimethylsiloxane (PDMS) stamp (see scheme in Figure 1a), which upon thermolysis at 195 °C led to nanocrystalline Pd μ-stripes inside the microchannels (nanoparticle size, 8 ± 2 nm, see the Supporting Information, Figure S1). As is well-known, polyimide can easily withstand such temperatures without losing its flexibility.[35] Although the thermolysis of the precursor is expected to remove the hydrocarbon by desorption,[36] depending on the temperature, some amount of carbon is usually left behind (see the Supporting Information, Table S1). For the 195 °C treatment, it is as high as 58.6 at %. In this sense, the Pd μ-stripes are nanocomposites of Pd nanoparticles in carbon matrix (vide infra). The formed μ-stripes were ~1.1 μm wide with a spacing of ~400 nm, in conformity with the PDMS mold (Figure 1b). A pair of Au electrodes was deposited onto the μ-stripes by shadow

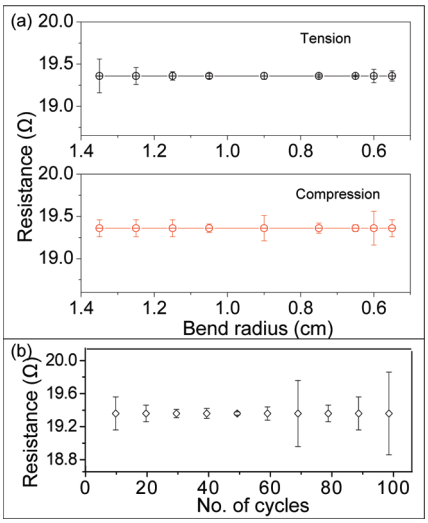

Figure 3. Pd μ-stripes obtained from 230 °C thermolysis exhibiting near constant resistance (a) for different bend radii under tension and compression and (b) over many cycles at a tensile bend radius of 1.1 cm. The error bars stands for the changes in the resistance value during the measurement.

masking such that as many as ∼7500 stripes ran perpendicular to the 6 μm gap (Figure 1c). Figure 1d shows a photograph of the fabricated flexible strain sensor device with μ-stripes exhibiting brilliant colors in ambient light because of diffraction.

The resistance of the sensor device was measured in the ambient at room temperature for varying bent radius, under both tension and compression (Figures 2a and b). With the device held flat, the collective resistance of the stripes was 4.34 MΩ. When the μ-stripes were subjected to tensile strain (Figure 2a), with the bending radius decreasing from ∞ (flat) to below 0.5 cm, the resistance of the device gradually increased to 6.82 MΩ, as shown in Figure 2c. On the other hand, under compressive strain, the resistance of the device decreased gradually to 2.48 MΩ also shown in Figure 2c. The release of either strain brought the device back to its original flat position with characteristic resistance. The change in resistance expressed as normalized values are shown in Figure 2d against % strain for the μ-stripes obtained by thermolysis at 195 °C. The slope of the plot is the gauge factor that defines the performance of the sensor device. For the data shown in Figure 2d, the gauge factor was estimated to be ∼390 for tensile strain and ∼249 for compressive strain, which are commendable values. The gauge factor values obtained from the μ-stripes are considerably higher compared to conventional metal and alloy strain gauges (1−5). Further, the sensor is remarkably sensitive to even small strains like ∼0.09%. Low temperature conductance measurements revealed the activation energy for the transport to be ∼25 meV (see the Supporting Information, Figure S2). This value is in line with the activation energies obtained for metal-containing diamond-like-carbon films.[37]

Here we relate the results obtained for sensors produced with different thermolysis temperature. Higher temperatures (230−250 °C) produce metallic stripes[34] with conductivity close to that of the bulk Pd, with only a little carbon left behind (see the Supporting Information, Table S1, and ref 34). When molding was carried out on the flexible substrate, the obtained stripes were metallic as expected but interestingly, showed no response to

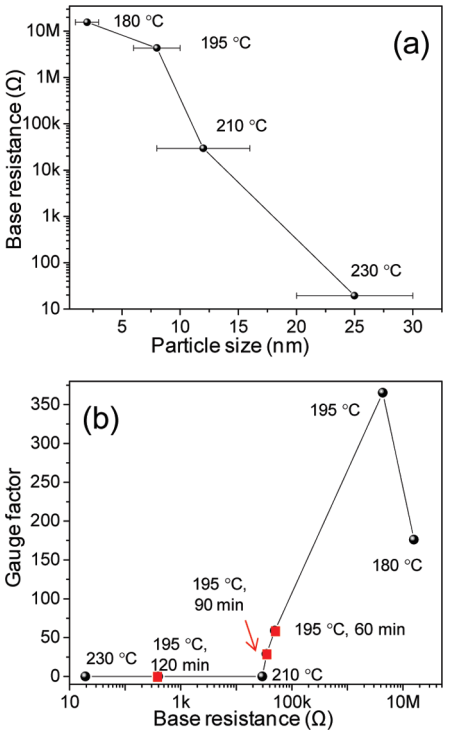

Figure 4. (a) Strain sensor base resistance (resistance while being flat) vs Pd particle size in μ-stripes. (b) Gauge factor as a function of the base resistance of Pd μ-stripes. The thermolysis temperatures used for producing the stripes are indicated alongside (time, 30 min). Three data points (squares) in (b) refer to thermolysis at 195 °C for 60, 90, and 120 min.

bending. Indeed, with either strain, the resistance remained nearly constant at its base value (19.4 ± 0.2 Ω) (Figure 3a). Interestingly, the μ-stripes were stable even after 100 cycles of bending (Figure 3b). This observation is well contrasting with the sensor action shown in Figure 2.

We have observed in separate experiments that the stripes produced with thermolysis temperatures in the range 195−230 °C were poorly conducting and exhibited little response to strain (see the Supporting Information, Figure S3). The stripes obtained from a 180 °C treatment were not only highly insulating but also were poorly sensing the strain (see the Supporting Information, Figure S4). These results are shown in Figure 4 and discussed below.

As shown in Figures 2 and 3, the temperature of thermolysis decides the electrical property of the μ-stripes and thus the sensing ability. Thermolysis influences the constitution of the μ-stripe in two ways, namely, the Pd nanoparticle size and the nature of the carbon matrix that is left behind after thermolysis. The decomposition of Pd thiolate[38] occurs by reductive elimination of thiol molecules leaving behind Pd as revealed by thermogravimetric analysis (see Figure S5 in the Supporting Information). The thiol molecules essentially undergo homolytic dissociation and desorb as disulfide molecules.[38] However, when the temperature is not high enough, partial decomposition may be expected where Pd nanoparticles are to be found amidst carbonaceous species, as shown by Raman measurements as well as by SEM and STEM (see Figure S6 in the Supporting Information). Thus at 195 °C, only small nanoparticles are produced (∼6−10 nm, see the Supporting Information ,Figure S1).

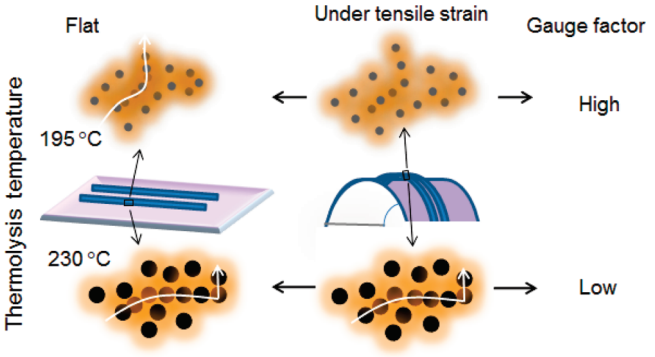

Figure 5. Schematic showing the Pd nanoparticle environment in the μ-stripes patterned on a polyimide shown on flat and bent substrates. Lower thermolysis results in smaller Pd particles surrounded with less conducting carbon species. Although there may be higher number of conducting paths (shown by white arrow), they easily break open under tensile strain. The opposite situation may be considered for compression strain. Higher thermolysis temperatures give rise to bigger particles with well-conducting carbon. In this case, the conducting paths are less affected during strain.

There is discernible contrast between SEM and STEM images from this sample, although individual nanoparticles could not be made out in carbon matrix due to the small size (see the Supporting Information, Figure S6b, c). Further, at this temperature the hydrocarbon decomposition appears to be incomplete and as a result, the overall carbon content remains comparable to the precursor state itself (58.6 at %, see the Supporting Information, Table S1). As seen from the Raman spectrum (see the Supporting Information, Figure S6a), there is considerable intensity associated with the D-band, related to the degree of disorder from the sp^3-hybridized carbon[39,40] which is essentially nonconducting. The particle size increased dramatically with the thermolysis temperature while the resistance of the stripes decreased (Figure 4a). Thus, the μ-stripes exhibit a wide range of resistance depending on the thermolysis temperature. The stripes resulting from the 230 °C thermolysis are essentially metallic (~19.3 Ω, Figure 2d) and exhibited no change in resistance with change in bend radius which means that the gauge factor is zero in this case. These properties owe much to the bigger Pd nanoparticles (~20−30 nm, see the Supporting Information, Figure S1) and less carbon (37.7 at %), a good fraction of it being sp^2 as evident from the Raman data (see the Supporting Information, Figure S6a). The intensity increase of the G peak originates from the formation of conductive sp^2 carbon atoms resulting in higher conductivity.[40] The presence of carbon around the Pd nanoparticles is clearly seen from the STEM images (see the Supporting Information, Figure S6d). This is also evident in the case of 210 °C treated sample (see the Supporting Information, Figure S7).

The stripes resulting from the 210 °C thermolysis exhibit a slightly higher resistance (20 kΩ) than those obtained from 230 °C thermolysis, as the metal particles are relatively smaller, ~8−16 nm (see Figure 4a). The surrounding carbon may be less sp^2 in nature. Interestingly, the applied strain has only little influence on their resistance with the estimated gauge factor of 0.11 (see Figure 4b). The thermolysis time also seems to have an influence of the particle size and the nature of carbon (see square data points in Figure 4b). Among the different samples, when the time duration was increased from 30 min to 60, 90, and 120 min at 195 °C, the base resistance decreased to 49.3, 35.0, and 0.39 kΩ, respectively, with corresponding gauge factors of 59, 29, and 0.1. Given the constitution of these μ-stripes, the strain seems to induce a change in the electronic coupling between the nanoparticles. With the μ-stripes obtained from the 195 °C thermolysis, the scenario is so well set with the nanoparticle size and the nature and content of carbon that the electronic coupling becomes most sensitive to any tiny change in the nanoparticle environment (see schematic illustration in Figure 5). This is relatively more expressed in the tensile strain as the nanoparticles move away from each other and the coupling becomes weaker. In the compressive regime, the nanoparticles are forced to come closer, which because of the surrounding carbon matrix is hindered more so at very short distances. This observation is in line with Vossmeyer et al.,[29] who found that the tensile strain brought larger changes in resistance than compressive strain in the case of Au nanoparticle networks. This was attributed to the dislocations which are produced when the interparticle distance can no longer be buffered by the organic material between the metal cores. Steric repulsion and other interactions may dominate this regime. If the base resistance becomes even higher as in the case of stripes resulting from 180 °C (see Figure 4), the interparticle coupling is nearly lost making the sensing action less effective, as the particle size for this sample is much smaller, ~2 ± 1 nm (see TEM image in Figure S1c in the Supporting Information). The results presented here may be compared with a strain sensor from the literature which was based on tungsten nanoparticles embedded in amorphous carbon.[41] In the latter, decreasing metal density of nanoparticles led to an increase in the gauge factor, the maximum value being 30. Another important aspect is the μ-stripe/electrode interface. In a strain sensor, ohmic contact of the electrodes with sensing elements is highly desirable[42] so that the observed changes in resistance arise mainly from the sensing element without the influence of the contacts. In our case, i.e., Pd μ-stripes, the linear $I-V$ characteristics (see the Supporting Information, Figure S8) obtained are typical of an ohmic contact. In the case of sample treated at 230 °C, which led to highly conducting Pd μ-stripes (results shown in Figure 3), the resistance did not change with bending, the standard deviation being less than ~0.2 Ω for different bend radii (Figure 3a), clearly indicating the reliability of the contacts. As the Au electrodes were made by the same method in all cases (by thermal evaporation of Au onto the stripes), the contacts should be similar in all cases.

Instead of μ-stripes, films derived from thermolysis at 195 °C have been tried out (see Figure S9 in the Supporting Information). Although the film exhibited a comparable resistance value as the μ-stripes, the obtained gauge factor was way below (0.1). This observation emphasizes the importance of molding the sensor element in the form of μ-stripes. The confinement of the material in the latter perhaps leads to a better translation of the strain into change in resistance. The summary of the strain sensors fabricated in the present study is given in Table 1.

Table 2 lists the performance parameters of typical strain sensors reported in the literature. For example, a strain sensor based on a single SWNT exhibited gauge factor of 269 at a working voltage of 5 V.[28] ZnO nanorod -based strain sensor with very high gauge factor was found to operate at 2 V (see Table 2).[32] In contrast, the sensor reported in this study typically works at 0.2 V. The fabrication process is also of course much simpler. Another noteworthy feature is that the temperature

Table 1. Summary of Strain Sensors Fabricated in the Present Study (Thermolysis time is fixed to be 30 min unless mentioned)

S. no.	thermolysis temperature (°C)		particle size (nm)	base resistance (Ω)	gauge factor
1	180		2	15.68M	176
2	195	30 min	8	4.34M	390
3		60 min		49.3K	59
4		90 min		35K	29
5		120 min		393	0.1
6	210		12	29.5K	0.11
7	230		25	19.3	0

Table 2. Comparative Study of Typical Two-Terminal Strain Gauge Sensors Reported in the Literature

material	maximum working range of strain (%)	gauge factor	operating voltage/range (V)	ref
Ni wire (commercial)	0.15	~2	6	43
Piezoresistive doped nanocrystalline Si	0.2	30	5	44
Si nanowire	3	~ 20	~3	45
ZnO nanowire	1.2	1250	~2	3
ZnO nanorod	1.4	6.7×10^8	2	32
Piezoresistive carbon filament	1.5	~ 10	~2.4	46
MWCNT/epoxy composite	2	~ 75	10	47
SWNT	0.08	210	0.05	48
SWNT	0.24	269	5	28
Pd μ-stripes	0.22	390	0.2	present work

coefficient of resistance for our sensor (see the Supporting Information, Figure S10) is around 0.00228 K^{-1}, lower than the bulk Pd (0.00572 K^{-1}). Thus, temperature variations in the ambient will have little effect on the performance of the sensor.

In conclusion, the above study has shown how a practically useful strain gauge sensor may be produced based on Pd μ-stripe grating structures.[49] The merit lies in the simple process of direct micromolding with well controlled electrical properties which in turn give a control on the gauge factor itself. Here, the decomposition chemistry of the Pd alkanethiolate precursor plays a key role. By thermolysing the molded stripes at 230 °C, we have been able to produce well-conducting Pd μ-stripes (zero gauge factor) which are robust and can withstand bending over many cycles with resistance unchanged. This corresponds to a situation where the Pd nanoparticles are well coupled with little carbon around. Such highly conducting stripes may find applications as flexible electrodes. By thermolysing at 195 °C on the other hand, we have produced high-resistance stripes with gauge factor greater than ~300. The sensor action is primarily derived from the changing coupling between the Pd nanoparticles in the carbon matrix. The confinement of the materials in the form of μ-stripes seems important; a film obtained under similar thermolysis conditions, shows only a small gauge factor (0.1). Clearly, the strain sensor reported here is comparable to the existing commercial metallic strain gauges in terms of working range of strains, and superior in terms of the gauge factor. Comparing with the sensors based on nanomaterials, the employed fabrication process is much simpler and inexpensive (see the Supporting Information, Figure S11) and requires neither high-temperature processing nor sophisticated equipment. Thus, it is a direct, single-step, solution-based process with good control over the electronic property of the strain sensor element. As the sensor is highly flexible, it can easily adapt to any surface topology and the base resistance may be redefined for the assumed shape. Further, the substrate (polyimide) with the μ-stripe grating structure on top possesses favorable transparency in the visible range (see dashed square regions in the abstract graphic). A strain sensor being transparent may offer additional advantages, particularly in transparent electronics.

EXPERIMENTAL SECTION

PDMS stamps were fabricated by replica molding on a commercially available compact disk (Sony CD-R). PDMS was prepared by mixing Sylgard 184 curing agent (Dow Corning) and its elastomer in the ratio of 1:10. The mixture was then degassed under a vacuum for 30 min. PDMS was poured onto the master (CD) and then cured in an oven at 60 °C overnight. PDMS stamps were cleaned using hexane and sonicated in ethanol to remove any uncured oligomers. The resulting stamp hosted relief features of width 505 nm with intermediate channels of 950 nm width. A flexible polyimide (~20 μm thick) was used as a substrate for molding Pd μ-stripes. Polyimide was cleaned by sonicating in acetone, isopropyl alcohol and double-distilled water and dried under flowing argon. The synthesis procedure for the precursor, Pd hexadecylthiolate, $Pd(SC_{16}H_{33})_2$, is reported elsewhere.[36] Approximately 60 μL of the precursor solution (10 mM in toluene) was dropped at one edge of the stamp kept on the substrate to fill the channels spontaneously by capillary action. The set up was gradually heated on a hot plate to reach the desired temperature (180, 195, 210, or 230 °C) and was held for 30 min. Following cooling to room temperature, the stamp was removed leaving behind the patterns on the substrate. The patterned substrates were examined using a Nova NanoSEM 600 instrument (FEI Co., The Netherlands). Au contact pads were deposited using a shadow mask of 6 μm width. The resistive evaporation was done using a thin film deposition system (HindHi Vac., Bangalore) at a base pressure of 1×10^{-6} Torr.

Metallic contacts were drawn from the Au pads using silver epoxy (SPI suppliers, USA) and the resistance measurements were done using a digital multimeter (TestLink) with computer control.

■ ASSOCIATED CONTENT

Supporting Information. (1) TEM images of Pd nanoparticles, (2) Table showing carbon content among various samples thermolyzed at different temperatures, (3) Raman spectra of the carbon matrix, (4) strain sensing results from the control experiment of thermolyzed Pd film. This material is available free of charge via the Internet at http://pubs.acs.org/.

■ AUTHOR INFORMATION

Corresponding Author
*E-mail: kulkarni@jncasr.ac.in.

■ ACKNOWLEDGMENT

The authors thank Professor C. N. R. Rao for encouragement. Support from DST is acknowledged. The authors acknowledge Venkatasrinu Bhadram for help in Raman measurements. R.B. thanks CSIR and A.A.S. thanks DST for their fellowships.

■ REFERENCES

(1) Reuss, R. H.; Chalamala, B. R.; Moussessian, A.; Kane, M. G.; Kumar, A.; Zhang, D. C.; Rogers, J. A.; Hatalis, M.; Temple, D.; Moddel, G.; et al. *Proc. IEEE* **2005**, *93*, 1239.
(2) Window, A. L. *Strain Gauge Technology*, 2nd ed.; Elsevier Applied Science: Essex, U.K., 1992.
(3) Zhou, J.; Gu, Y.; Fei, P.; Mai, W.; Gao, Y.; Yang, R.; Bao, G.; Wang, Z. L. *Nano Lett.* **2008**, *8*, 3035.
(4) Laukhina, E.; Pfattner, R.; Ferreras, L. R.; Galli, S.; Mas-Torrent, M.; Masciocchi, N.; Laukhin, V.; Rovira, C.; Veciana, J. *Adv. Mater.* **2010**, *22*, 977.
(5) Park, S. I.; Le, A. P.; Wu, J.; Huang, Y.; Li, X.; Rogers, J. A. *Adv. Mater.* **2010**, *22*, 3062.
(6) Lee, K. J.; Meitl, M. A.; Ahn, J. H.; Rogers, J. A.; Nuzzo, R. G.; Kumar, V.; Adesida, I. *J. Appl. Phys.* **2006**, *100*, 124507.
(7) Kim, B. J.; Jang, H.; Lee, S.-K.; Hong, B. H.; Ahn, J.-H.; Cho, J. H. *Nano Lett.* **2010**, *10*, 3464.
(8) Sun, Y.; Kim, S.; Adesida, I.; Rogers, J. A. *Appl. Phys. Lett.* **2005**, *87*, 1.
(9) Tiwari, A. N.; Romeo, A.; Baetzner, D.; Zogg, H. *Prog. Photovolt: Res. Appl.* **2001**, *9*, 211.
(10) Liu, Z.; Subramania, V.; Misra, M. *J. Phys. Chem. C* **2009**, *113*, 14028.
(11) Tong, L.; Li, C.; Chen, F. e.; Bai, H.; Zhao, L.; Shi, G. *J. Phys. Chem. C* **2009**, *113*, 7411.
(12) Yun, J.; Cho, K.; Park, B.; Park, B. H.; Kim, S. *J. Mater. Chem.* **2009**, *19*, 2082.
(13) Choi, D.; Choi, M.-Y.; Shin, H.-J.; Yoon, S.-M.; Seo, J.-S.; Choi, J.-Y.; Lee, S. Y.; Kim, J. M.; Kim, S.-W. *J. Phys. Chem. C* **2009**, *114*, 1379.
(14) Choi, D.; Choi, M. Y.; Choi, W. M.; Shin, H. J.; Park, H. K.; Seo, J. K.; Park, J.; Yoon, S. M.; Chae, S.; Lee, Y. H.; et al. *Adv. Mater.* **2010**, *22*, 2187.
(15) Takahashi, T.; Takei, K.; Adabi, E.; Fan, Z.; Niknejad, A. M.; Javey *ACS Nano* **2010**, *4*, 5855.
(16) Hu, L.; Yuan, W.; Brochu, P.; Gruner, G.; Pei, Q. *Appl. Phys. Lett.* **2009**, *94*, 161108.
(17) Gomez De Arco, L.; Zhang, Y.; Schlenker, C. W.; Ryu, K.; Thompson, M. E.; Zhou, C. *ACS Nano* **2010**, *4*, 2865.
(18) Ahn, J. H.; Kim, H. S.; Lee, K. J.; Jeon, S.; Kang, S. J.; Sun, Y.; Nuzzo, R. G.; Rogers, J. A. *Science* **2006**, *314*, 1754.
(19) Xu, F.; Lu, W.; Zhu, Y. *ACS Nano* **2011**, *5*, 672.
(20) Kang, I.; Schulz, M. J.; Kim, J. H.; Shanov, V.; Shi, D. A. *Smart Mater. Struct.* **2006**, *15*, 737.
(21) Anderson, J. C. *J. Vac. Sci. Technol., A* **1986**, *4*, 610.
(22) Chiriac, H.; Urse, M.; Rusu, F.; Hison, C.; Neagu, M. *Sens. Actuators, A* **1999**, *76*, 376.
(23) Lichtenwalner, D. J.; Hydrick, A. E.; Kingon, A. I. *Sens. Actuators, A* **2007**, *135*, 593.
(24) Chung, D. D. L. *Smart Mater. Struct.* **1995**, *4*, 59.
(25) Lisong, Z.; Soyoun, J.; Brandon, E.; Jackson, T. N. *IEEE Trans. Electron Devices* **2006**, *53*, 380.
(26) Latessa, G.; Brunetti, F.; Reale, A.; Saggio, G.; Di Carlo, A. *Sens. Actuators, B* **2009**, *139*, 304.
(27) Takamatsu, S.; Takahata, T.; Muraki, M.; Iwase, E.; Matsumoto, K.; Shimoyama, I. *J. Micromech. Microeng.* **2010**, *20*, 075017.
(28) Chang, N. K.; Su, C. C.; Chang, S.-H. *App. Phys. Lett.* **2008**, *92*, 063501.
(29) Vossmeyer, T.; Stolte, C.; Ijeh, M.; Kornowski, A.; Weller, H. *Adv. Func. Mater.* **2008**, *18*, 1611.
(30) Siffalovic, P.; Chitu, L.; Vegso1, K.; Majkova, E.; Jergel, M.; Weis, M.; Luby, S.; Capek, I.; Keckes, J.; Maier, G. A.; et al. *Nanotechnology* **2010**, *21*, 385702.
(31) Mueggenburg, K. E.; Lin, X.-M.; Goldsmith, R. H.; Jaeger, H. M. *Nat. Mater.* **2007**, *6*, 656.
(32) Liu, N.; Fang, G.; Zeng, W.; Long, H.; Yuan, L.; Zhao, X. *J. Phys. Chem. C* **2011**, *115*, 570.
(33) Gullapalli, H.; Vemuru, V. S. M.; Kumar, A.; Botello-Mendez, A.; Vajtai, R.; Terrones, M.; Nagarajaiah, S.; Ajayan, P. M. *Small* **2010**, *6*, 1641.
(34) Radha, B.; Kulkarni, G. U. *Small* **2009**, *5*, 2271.
(35) Tiwari, A. N.; Krejci, M.; Haug, F. J.; Zogg, H. *Prog. Photovolt: Res. Appl.* **1999**, *7*, 393.
(36) Bhuvana, T.; Kulkarni, G. U. *ACS Nano* **2008**, *2*, 457.
(37) Takeno, T.; Hoshi, Y.; Miki, H.; Takagi, T. *Diamond Relat. Mater.* **2008**, *17*, 1669–1673.
(38) (a) Nakamoto, M.; Yamamoto, M.; Fukusumi, M. *Chem. Commun.* **2002**, 1622. (b) Carotenuto, G.; Martorana, B.; Perlo, P.; Nicolais, L. *J. Mater. Chem.* **2003**, *13*, 2927.
(39) Goryainova, S. V.; Pan, Y.; Madyukov, I. A. *Bull. Russ. Acad. Sci.* **2009**, *73*, 874.
(40) Cai, Y.; Wolfkuhler, D.; Myalitsin, A.; Perlich, J.; Meyer, A.; Klinke, C. *ACS Nano* **2011**, *5*, 67.
(41) Ohno, T.; Takeno, T.; Miki, H.; Takagi, T. *Int. J. Appl. Electromagn. Mech.* **2010**, *33*, 665.
(42) Han, X.; Jing, G.; Zhang, X.; Ma, R.; Song, X.; Xu, J.; Liao, Z.; Wang, N.; Yu, D. *Nano Res.* **2009**, *2*, 553.
(43) IPA Pvt Ltd, Bangalore (http://ipaindia.com/)
(44) Alpuim, P.; Filonovich, S. A.; Costa, C. M.; Rocha, P. F.; Vasilevskiy, M. I.; Lanceros-Mendez, S.; Frias, C.; Marques, A. T.; Soares, R.; Costa, C. *J. Non-Cryst. Solids* **2008**, *354*, 2585.
(45) Xu, F.; Durham, J. W.; Wiley, B. J.; Zhu, Y. *ACS Nano* **2011**, *5*, 1556.
(46) Xiaoping, S.; Chung, D. D. L. *Smart Mater. Struct.* **1996**, *5*, 243.
(47) Wichmann, M. H. G.; Buschhorn, S. T.; Boger, L.; Adelung, R.; Schulte, K. *Nanotechnology* **2008**, *19*, 475503.
(48) Stampfer, C.; Helbling, T.; Obergfell, D.; Schoberle, B.; Tripp, M. K.; Jungen, A.; Roth, S.; Bright, V. M.; Hierold, C. *Nano Lett.* **2006**, *6*, 233.
(49) Importantly, the precursor enables patterning by e-beam,[36] and inkjet printing, in addition to molding (see Bhuvana, T.; Boley, W.; Radha, B.; Dolash, B. D.; Chiu, G.; Bergstrom, D.; Reifenberger, R.; Fisher, T. S.; Kulkarni, G. U. *Micro Nano Lett.* **2010**, *5*, 296)..